Chinese Chemical Letters 36 (2025) 110191

Contents lists available at ScienceDirect

Chinese Chemical Letters

journal homepage: www.elsevier.com/locate/cclet

Lipid droplets and gallbladder targeted fluorescence probe for ratiometric NO imaging in gallstones disease models

Zhoupeng Zheng, Shengyi Gong, Qianhua Li, Shiya Zhang, Guoqiang Feng*

Key Laboratory of Pesticide & Chemical Biology of Ministry of Education, Engineering Research Center of Photoenergy Utilization for Pollution Control and Carbon Reduction, Ministry of Education, College of Chemistry, Central China Normal University, Wuhan 430079, China

ARTICLE INFO

Article history:
Received 10 May 2024
Revised 25 June 2024
Accepted 27 June 2024
Available online 27 June 2024

Keywords:
Ratiometric fluorescent probe
Nitric oxide
Lipid droplets
Gallbladder
Gallstone disease

ABSTRACT

Gallstones are a common disease worldwide, often leading to obstruction and inflammatory complications, which seriously affect the quality of life of patients. Research has shown that gallstone disease is associated with ferroptosis, lipid droplets (LDs), and abnormal levels of nitric oxide (NO). Fluorescent probes provide a sensitive and convenient method for detecting important substances in life systems and diseases. However, so far, no fluorescent probes for NO and LDs in gallstone disease have been reported. In this work, an effective ratiometric fluorescent probe **LR-NH** was designed for the detection of NO in LDs. With an anthracimide fluorophore and a secondary amine as a response site for NO, **LR-NH** exhibits high selectivity, sensitivity, and attractive ratiometric capability in detecting NO. Importantly, it can target LDs and shows excellent imaging ability for NO in cells and ferroptosis. Moreover, **LR-NH** can target the gallbladder and image NO in gallstone disease models, providing a unique and unprecedented tool for studying NO in LDs and gallbladder.

Gallstones are a prevalent global disease, up to 20% of adults develop gallstones [1,2]. Various risk factors, such as age, pregnancy, lack of exercise, obesity, and overnutrition, contribute to the formation of gallstones [2]. Impaired gallbladder emptying leading to cholestasis is considered a fundamental dynamic factor in gallstone formation [3]. Furthermore, bile stasis caused by gallstones can lead to inflammatory changes in the bile ducts, ultimately progressing to Cholangiocarcinoma. Throughout this process, there is an exacerbation of iron-dependent oxidative stress, with ferroptosis playing a role [4,5]. Nitric oxide (NO), as an important gaseous signal mole, plays a vital role in living organisms. It is a relaxation factor [6,7], and is closely related to intercellular communication, neurotransmission, cardiovascular, gastrointestinal, urogenital system, respiratory system, anti-pathogenicity, anti-tumor response and oxidative stress, and so on [8]. Notably, NO is an important neurotransmitter, which is abundant in the sphincter of Oddi and regulates biliary movement [9,10]. This means that the course of gallstones might be accompanied by changes in NO levels. On the other hand, in patients with gallstones, the accumulation of lipid droplets (LDs) leads to adipocyte hypertrophy [11]. Therefore, the detection of NO in LDs, ferroptosis, and gallstone disease is of great significance.

Fluorescent probes, known for their high sensitivity, good biocompatibility, and ability to perform real-time non-invasive detection, have been widely employed in biological imaging [12-16]. Ratiometric fluorescence probes, capable of self-tuning between two fluorescence bands, effectively overcome issues related to probe concentration, pH value, instrument efficiency, and temperature, making them particularly useful for the detection of important substances in living organisms [17-22]. Meanwhile, organelle-targeted fluorescent probes provide a more precise imaging tool for understanding changes in important substances within cells [23-25]. So far, although many excellent NO probes have been reported [26-30], organelle-targeted ratiometric fluorescent probes for NO are rarely reported [31-33]. Particularly, the development of a lipid droplet-targetable fluorescent probe for ratiometric imaging of NO remains unexplored.

Here, we report a readily obtainable fluorescent probe (**LR-NH**, Scheme 1) for ratiometric imaging of NO in LDs. The probe uses an anthracimide as the fluorophore and a secondary amine as the NO reaction site [34]. The fluorophore contains a hydrophobic *n*-octyl carbon chain, giving the probe **LR-NH** a lipophilic structure and allowing it to target LDs. Our results show that **LR-NH** exhibits rapid, colorimetric, and ratiometric fluorescence changes for NO with high selectivity and sensitivity. Moreover, **LR-NH** can effectively target LDs and image both exogenous and endogenous NO in living cells. **LR-NH** also shows the ability to image the level

* Corresponding author.
E-mail address: gf256@mail.ccnu.edu.cn (G. Feng).

https://doi.org/10.1016/j.cclet.2024.110191
1001-8417/

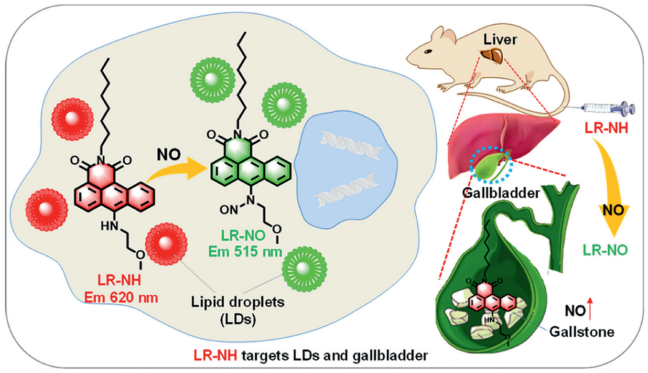

Scheme 1. Probe **LR-NH** for the ratiometric fluorescent detection of NO in lipid droplets and gallstones disease.

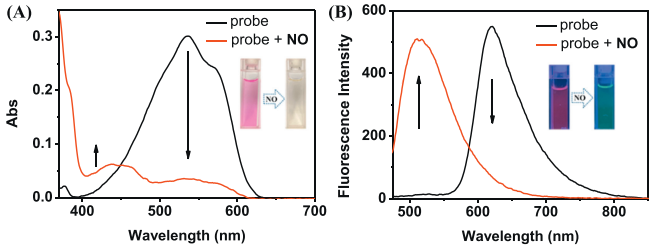

Fig. 1. (A) UV–vis and (B) fluorescent spectral changes of **LR-NH** (10 μmol/L) before and after adding NO (35 μmol/L) in phosphate buffered saline (PBS) buffer (10 mmol/L, pH 7.4, 30% CH_3CN, v/v). λ_{ex} = 460 nm. Inset in (A) and (B): The color change and emission color change, respectively.

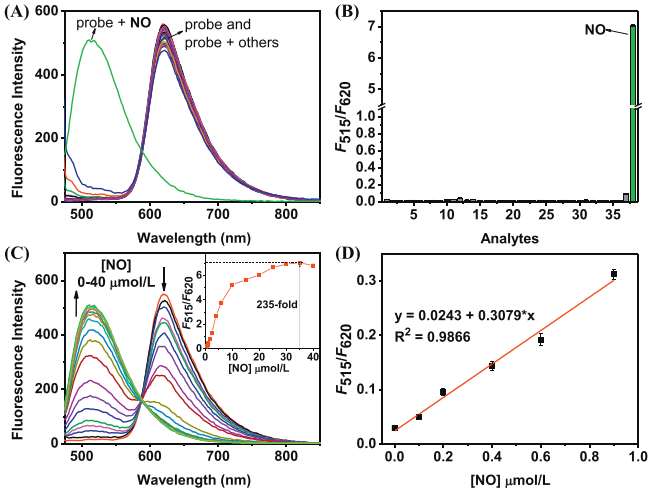

Fig. 2. (A) Fluorescence and (B) intensity ratio F_{515}/F_{620} changes of **LR-NH** (10 μmol/L) toward various analytes (each 100 μmol/L, except: GSH, 1 mmol/L; NO, 35 μmol/L) including 1–38: none, Br^-, Cl^-, F^-, I^-, HCO_3^-, HSO_3^-, SO_4^{2-}, K^+, Ca^{2+}, Zn^{2+}, Mg^{2+}, Fe^{3+}, Fe^{2+}, L-Arg, Ala, Phe, Ser, Val, Trp, Thr, Lys, AA, DHA, MGO, GSH, Hcy, Cys, H_2O_2, ClO^-, $ONOO^-$, NO_3^-, NO_2^-, $O_2^{\bullet-}$, HNO, $ROO^{\bullet}$, $^{\bullet}OH$, and NO. (C) Spectral changes of 10 μmol/L **LR-NH** to 0–40 μmol/L of NO. Inset: The change of F_{515}/F_{620} against the NO concentrations. (D) Linear response of F_{515}/F_{620} to 0–0.9 μmol/L of NO. λ_{ex} = 460 nm. Error bars in (B) and (D) represent mean deviation (±S.D.), n = 3.

changes of NO during cellular inflammation and ferroptosis. More importantly, **LR-NH** can target the gallbladder and image NO in gallstone disease models. To our knowledge, **LR-NH** is the first probe that enables ratiometrically imaging of NO in LDs and gallbladder (Table S1 in Supporting information).

LR-NH was synthesized according to Scheme S1 (Supporting information) and the characterization data were listed in Figs. S1–S6 (Supporting information). After obtaining **LR-NH**, its spectra before and after the addition of NO were explored (Fig. 1). **LR-NH** shows a broad strong absorption band around 536 nm and strong fluorescence at 620 nm. After the addition of NO, this absorption band significantly decreased. Meanwhile, the fluorescence at 620 nm decreased and a new fluorescence peak at 515 nm emerged, resulting in a ratiometric fluorescence change with a remarkable blue shift (105 nm). Concurrently, the purple probe solution turned nearly colorless and the emission color turned from red to green. A time-dependent analysis of the fluorescence intensity changes before and after adding NO was performed (Fig. S7 in Supporting information). It was observed that **LR-NH** exhibited good stability before the addition of NO. However, after adding NO, the fluorescence at 620 and 515 nm rapidly decreased and increased, respectively, and saturation was reached within 5 min, indicating that **LR-NH** rapidly and ratiometrically responds to NO. Altogether, **LR-NH** is a rapid, colorimetric, and ratiometric fluorescent probe for NO.

LR-NH was exposed to a wide range of reactive species (NO, NO_3^-, NO_2^-, $O_2^{\bullet-}$, HNO, $ONOO^-$ ClO^-, $ROO^{\bullet}$, $^{\bullet}OH$, H_2O_2), amino acids (Arg, Ala, Phe, Ser, Val, Trp, Thr, Lys), and other species (F^-, Cl^-, Br^-, I^-, HCO_3^-, HSO_3^-, SO_4^{2-}, K^+, Ca^{2+}, Zn^{2+}, Mg^{2+}, Fe^{3+}, Fe^{2+}, ascorbic acid (AA), dehydroascorbic acid (DHA), methylglyoxal (MGO), glutathione (GSH), homocysteine (Hcy), and cysteine (Cys)) to assess its selectivity. As depicted in Fig. 2A, only NO leads to significant changes in **LR-NH** fluorescence. As a result, only NO induced obvious ratiometric fluorescence changes at 515/620 nm (Fig. 2B). Moreover, even with other analytes present, **LR-NH** showed significant ratiometric fluorescence changes for NO (Fig. S8 in Supporting information). These findings indicate that **LR-NH** can detect NO with high selectivity.

We also evaluated the sensitivity of **LR-NH** to NO. As depicted in Fig. 2C, when the concentration of NO gradually increases, the fluorescence of **LR-NH** at 620 nm and 515 nm progressively decreases and increases, respectively. The fluorescence ratio of F_{515}/F_{620} was directly correlated to the concentration of NO, and a maximum enhancement was found to be ~235-fold (from 0.03 to 7.04, see the inset of Fig. 2C) after the addition of 35 μmol/L of NO. Importantly, there is a linear relationship between the ratio of F_{515}/F_{620} and the NO concentration of NO (0–0.9 μmol/L) (Fig. 2D), which gives a low detection limit of 0.49 nmol/L (3σ/k method), indicating a high sensitivity of **LR-NH** for NO. Based on these results and relevant references [34,35], a corresponding reaction mechanism was proposed in Scheme S2 (Supporting information) to explain the fluorescence changes of **LR-NO** for NO. The product **LR-NO** was confirmed by high resolution mass spectrometry (HR-MS) (Fig. S9 in Supporting information), which supports this mechanism.

The influence of pH on the detection of NO was also investigated. As depicted in Fig. S10 (Supporting information), within the pH range of 3.0–11, the F_{515}/F_{620} of **LR-NH** remained stable in the absence of NO. However, after adding NO, the F_{515}/F_{620} exhibited a significant increase over a wide pH range (3.0–11) including the physiological pH range. This demonstrates that **LR-NH** can be utilized under physiological pH conditions.

To assess the cytotoxicity of **LR-NH**, the MTT method was employed on two cell lines (HeLa and RAW264.7 cells). The results indicated that even if the concentration of **LR-NH** was used up to 50 μmol/L, the cell survival rate after 24 h incubation was greater than 85% (Fig. S11 in Supporting information), suggesting that **LR-NH** exhibits low cytotoxicity.

We next evaluated the subcellular targeting ability of **LR-NH**. As Fig. 3 shows, living cells stained with **LR-NH** displayed many strong fluorescent red dots, which highly overlap with the fluorescence of the commercial LDs dye Lipid-tracker Green (Pear-

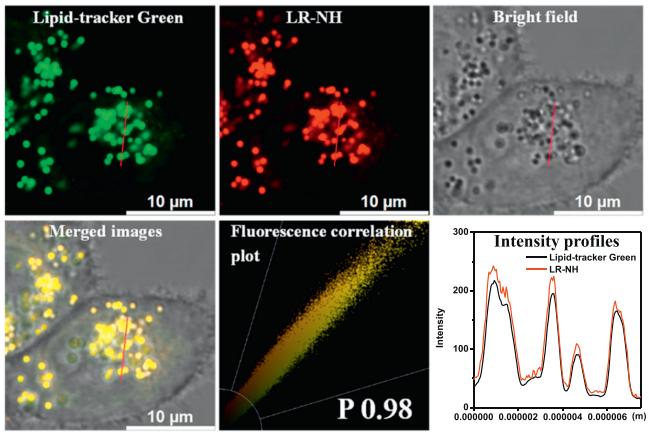

Fig. 3. HeLa cell images co-incubated with 0.2 μmol/L Lipid-tracker Green and 5 μmol/L **LR-NH** for 30 min. Lipid-tracker Green channel: $\lambda_{em}/\lambda_{ex}$ = 500–550 nm/488 nm. **LR-NH** channel: $\lambda_{em}/\lambda_{ex}$ = 590–660 nm/488 nm.

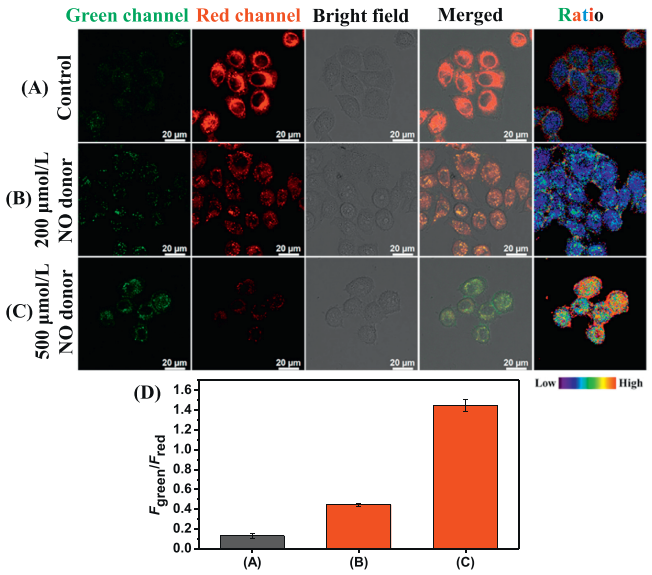

Fig. 4. Confocal fluorescence imaging of exogenous NO in HeLa cells with 5 μmol/L **LR-NH**. (A) **LR-NH** for 0.5 h, (B) **LR-NH** for 0.5 h, 200 μmol/L DEA·NONOate for 0.5 h. (C) **LR-NH** for 0.5 h, 500 μmol/L DEA·NONOate for 0.5 h. (D) Imaging quantification data of F_{green}/F_{red}. λ_{ex} = 488 nm. Fluorescence collected: Green channel 495–550 nm, red channel 590–660 nm. Error bars in (D) represent mean deviation (±S.D.), n = 3.

son's co-localization coefficient: 0.98). However, it was found that the fluorescence of **LR-NH** overlapped relatively poorly with other commercial organelle dyes, such as Lyso-tracker Green and Mito-tracker Green (Fig. S12 in Supporting information). These results suggest that **LR-NH** primarily targets lipid droplets.

Next, **LR-NH** was explored for NO imaging in living cells. The imaging of exogenous NO in HeLa cells was first studied. As depicted in Fig. 4, the cells treated with **LR-NH** exhibited strong red fluorescence but very weak green fluorescence (Fig. 4A). However, when the cells were added with the NO donor DEA·NONOate (200 and 500 μmol/L, respectively), the red fluorescence in cells decreased, meanwhile, the green fluorescence increased (Figs. 4B and C). Consequently, the fluorescence ratio of F_{green}/F_{red} showed a significant enhancement (from 0.13 to 1.45, Fig. 4D), indicating that **LR-NH** can effectively detect exogenous NO in living cells.

Then, the imaging of endogenous NO in RAW264.7 cells was conducted. In these experiments, endogenous NO production was stimulated by lipopolysaccharide (LPS) (and LPS + L-Arg) and inhibited by NG-monomethyl-L-arginine (L-NMMA). As shown in Fig. 5,

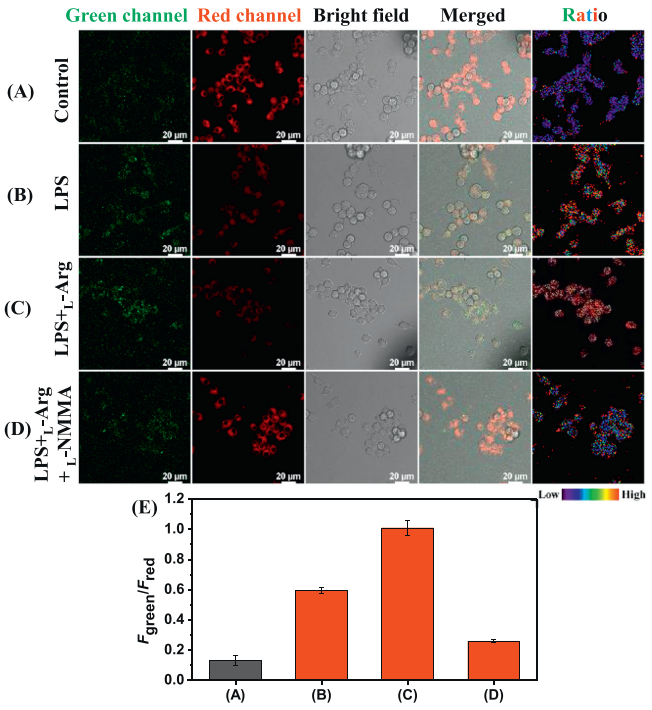

Fig. 5. Endogenous NO imaging with **LR-NH** (5 μmol/L). RAW264.7 cells were incubated with (A) **LR-NH** for 0.5 h, (B) LPS for 12 h then **LR-NH** for 0.5 h. (C) LPS, L-Arg for 12 h then **LR-NH** for 0.5 h. (D) LPS, L-Arg, L-NMMA for 12 h then **LR-NH** for 0.5 h. (E) Quantification of imaging data. λ_{ex} = 488 nm. Fluorescence collected: Green channel 495–550 nm, and red channel 590–660 nm. Error bars in (E) represent mean deviation (±S.D.), n = 3.

the cells treated with **LR-NH** only showed strong red fluorescence (control group). However, using LPS or LPS + L-Arg to treat cells and then staining with **LR-NH**, the red fluorescence inside the cells reduced significantly, while the green fluorescence enhanced significantly. In the L-NMMA treated group, as expected, there was no significant decrease in intracellular red fluorescence and no significant enhancement in green fluorescence. This indicates that endogenous NO can be imaged by **LR-NH**. With these results, we hence can conclude that **LR-NH** is a promising new probe that can be used for ratiometric fluorescent detecting endogenous and exogenous NO in LDs.

With the above results, we explored **LR-NH** to detect the level changes of NO during cell ferroptosis. As indicated in Fig. 6A, the control group displayed significant fluorescence in the red channel. Upon stimulation of cells with erastin to induce ferroptosis, green fluorescence increased while red fluorescence weakened, leading to a significant increase in the F_{green}/F_{red} ratio (Fig. 6B). When Fer-1 was added to inhibit the ferroptosis process, the F_{green}/F_{red} ratio fell between that of the control group and the erastin group (Fig. 6C). These findings indicate an increase in NO levels during the erastin-induced ferroptosis.

The excellent fluorescence imaging performance of **LR-NH** in living cells prompted us to further explore its applications *in vivo*. All the following mice experiments were approved by the Animal Ethical Experimentation Committee of Central China Normal University. Interestingly, when **LR-NH** was tail vein injected into mice, we found that the liver area showed significant fluorescence enhancement signals within 30 min (Figs. S13A and B in Supporting information). However, when the mice were dissected and their organs were removed for imaging, we found that the fluorescence came from the gallbladder rather than the liver (Figs. S13C and D in Supporting information). This indicates that **LR-NH** targets the gallbladder. It is worth noting that there are almost no reports in

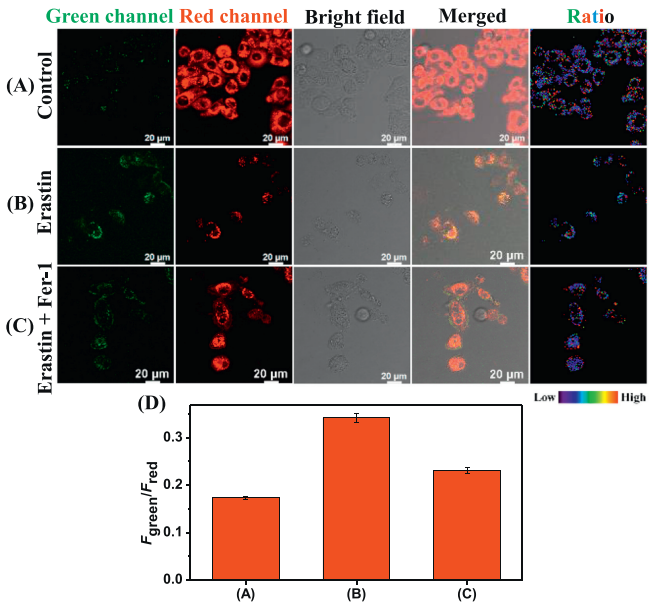

Fig. 6. Imaging of NO in erastin-induced ferroptosis. Cells were incubated with (A) **LR-NH** (5 μmol/L) for 0.5 h as the control group. (B) Erastin (10 μmol/L) for 6 h, and then **LR-NH** (5 μmol/L) for 0.5 h. (C) Erastin (10 μmol/L) and Fer-1 (10 μmol/L) for 6 h, and then **LR-NH** (5 μmol/L) for 0.5 h. (D) Imaging quantification data of F_{green}/F_{red}. λ_{ex} = 488 nm, fluorescence collected: Green channel 495–550 nm, red channel 590–660 nm. Error bars in (D) represent mean deviation (±S.D.), n = 3.

the literature on fluorescent probes that can locate the gallbladder. Therefore, **LR-NH** is a unique probe that can locate the gallbladder, providing the possibility for imaging the gallbladder and its related diseases. Considering that gallstone disease is very common, we established mouse gallstone models [36] and used **LR-NH** for imaging. As shown in Fig. S14 (Supporting information), unlike the normal group, obvious gallstone crystallizations were observed in the bile of the gallstone mouse model group, indicating that the gallstone model was successfully established. Then, the normal mice and gallstone disease mice were imaged with **LR-NH**. As depicted in Fig. S15 (Supporting information), when **LR-NH** was injected into the mice, both the normal (as control) and the gallstone mice showed obviously increased fluorescence at 620 nm in the gallbladder area, however, the gallstone control group displayed weaker fluorescence compared to the control group. Considering that **LR-NH** is sensitive to NO, this observation might suggest a higher concentration of NO in the gallstone mice group. However, due to the tissue penetration limitation of short-wavelength green fluorescence, we could not directly observe the changes in green fluorescence *in vivo*. So, we dissected the mice for imaging at two channels. As shown in Figs. 7A and B, the gallstone group showed weaker fluorescence at 620 nm but stronger fluorescence at 520 nm than the control group. These findings indicate that the level of NO increases in gallstone disease. The main organs were then isolated from the control group and the gallstone group for imaging at both green (520 nm) and red (620 nm) channels. As shown in Figs. 7C and D, indeed, fluorescence is concentrated in the gallbladder. Moreover, compared to the control group, the gallbladder in the gallstone group showed stronger fluorescence at 520 nm and weaker fluorescence at 620 nm. This indicates that **LR-NH** is a promising probe that can selectively image the gallbladder and detect the changes in NO concentration in the gallbladder.

In conclusion, we have successfully developed **LR-NH**, an LD-targetable fluorescent probe for ratiometric imaging of NO. **LR-NH** exhibits high selectivity and sensitivity for NO with remarkable ratiometric fluorescence changes at 515/620 nm and high LD-targeting ability. **LR-NH** also can detect both endogenous and exogenous NO in LDs and provides a promising new probe to ratiometrically image the level changes of NO during cellular inflammation and ferroptosis. Importantly, **LR-NH** can target the gallbladder to detect the level changes of NO in mouse gallstone models. It is worth noting that **LR-NH** is the first fluorescent probe that enables ratiometrically imaging of NO in LDs and gallbladder. Overall, this study provides an unprecedented tool for NO imaging in LDs and gallbladder-related diseases.

Declaration of competing interest

The authors declare that they have no known competing financial interests or personal relationships that could have appeared to influence the work reported in this paper.

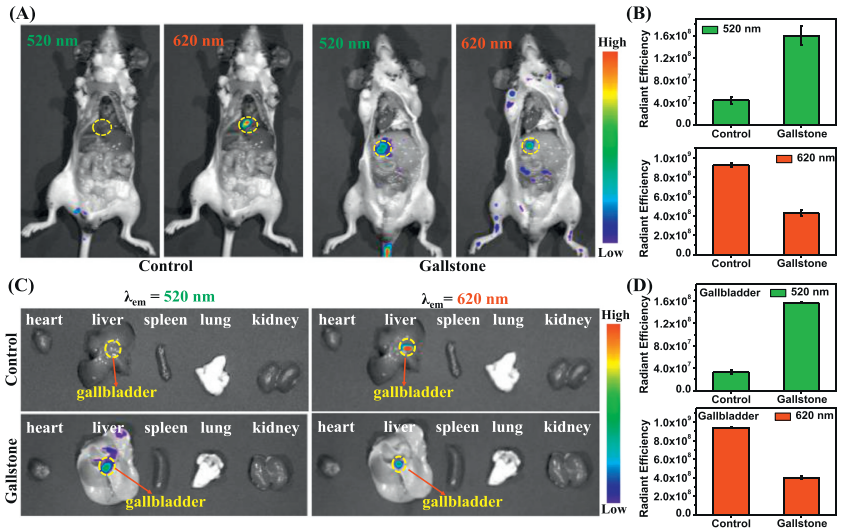

Fig. 7. (A) Fluorescence imaging of the control mice and the gallstone mice after 30 min of tail vein injection of **LR-NH** (100 μL, 200 μmol/L). Images were collected at 520 nm (Ex 480 nm) and 620 nm (Ex 540 nm) after dissection. (B) Fluorescence quantification analysis of the area circled by the yellow dashed line in (A). (C) Fluorescence imaging of the isolated heart, liver, spleen, lung, and kidney from the control mice and the gallstone mice. The yellow dashed line in the liver circles the gallbladder. Images were collected at 520 nm (Ex 480 nm) and 620 nm (Ex 540 nm). (D) Fluorescence quantification analysis of the gallbladder at 520 and 620 nm. Error bars in (B) and (D) represent mean deviation (±S.D.), n = 3.

CRediT authorship contribution statement

Zhoupeng Zheng: Writing – original draft, Methodology, Investigation, Formal analysis, Data curation. **Shengyi Gong:** Writing – review & editing, Formal analysis, Data curation. **Qianhua Li:** Writing – review & editing, Investigation, Formal analysis. **Shiya Zhang:** Writing – review & editing, Formal analysis. **Guoqiang Feng:** Writing – review & editing, Supervision, Project administration, Funding acquisition, Conceptualization.

Acknowledgments

This work was supported by the National Natural Science Foundation of China (No. 22077044) and the Natural Science Foundation of Hubei Province (No. 2022CFA033).

Supplementary materials

Supplementary material associated with this article can be found, in the online version, at doi:10.1016/j.cclet.2024.110191.

References

[1] F. Lammert, K. Gurusamy, C.W. Ko, et al., Nat. Rev. Dis. Primers. 2 (2016) 16024.
[2] X. Wang, W. Yu, G. Jiang, et al., Clin. Gastroenterol. Hepatol. 22 (2024) 1586–1595.
[3] J. Wei, Y. Wang, F. Du, et al., World J. Gastroenterol. 6 (2000) 102–106.
[4] J.Y. Han, K.S. Ahn, W.K. Baek, et al., Surg. Oncol. 34 (2020) 174–181.
[5] R. Thanan, S. Oikawa, P. Yongvanit, et al., Free Radical Biol. Med. 52 (2012) 1465–1472.
[6] B. Mayer, P. Andrew, Pharmacol. 358 (1998) 127–133.
[7] D. Fukumura, S. Kashiwagi, R.K. Jain, et al., Nat. Rev. Cancer 6 (2006) 521–534.
[8] D. Stuehr, J. Santolini, Z. Wang, et al., J. Biol. Chem. 279 (2004) 36167–36170.
[9] M.E. Simula, S.J. Brookes, A.C. Meedeniya, et al., Cell Tissue Res. 304 (2001) 31–41.
[10] M. Mourelle, F. Guarner, S. Moncada, et al., Gastroenterology 105 (1993) 1299–1305.
[11] M.M. Koch, U. Freddara, I. Lorenzini, et al., Digestion 18 (1978) 162–177.
[12] J. Lv, J. Gao, H. Li, et al., Chin. Chem. Lett. 35 (2024) 108940.
[13] W. Dou, H. Han, A. Sedgwick, et al., Sci. Bull. 67 (2022) 853–878.
[14] Y. Geng, Z. Wang, J. Zhou, et al., Chem. Soc. Rev. 52 (2023) 3873–3926.
[15] J. Ma, R. Sun, K. Xia, et al., Chem. Rev. 124 (2024) 1738–1861.
[16] C. Ding, T. Ren, Coord. Chem. Rev. 482 (2023) 215080.
[17] J. Li, Q. Qiao, Y. Ruan, et al., Chin. Chem. Lett. 34 (2023) 108266.
[18] K. Wang, L. Liu, D. Mao, et al., Angew. Chem. Int. Ed. 60 (2021) 15095–15100.
[19] Y. Qi, Y. Li, M. Tan, et al., Coord. Chem. Rev. 486 (2023) 215130.
[20] H. Jin, M. Yang, Z. Sun, et al., Coord. Chem. Rev. 446 (2021) 214114.
[21] Q. Fu, X. Yang, M. Wang, et al., ACS Nano 18 (2024) 3916–3968.
[22] S. Feng, J. Zheng, J. Zhang, et al., Sens. Actuator B: Chem. 371 (2022) 132512.
[23] L. Guo, M. Tian, Z. Zhang, et al., J. Am. Chem. Soc. 143 (2021) 3169–3179.
[24] L. Wang, Y. Zhang, M. Zheng, et al., Chem. Eng. J. 466 (2023) 143104.
[25] J. Hong, J. Zhang, Q. Li, et al., Anal. Chem. 95 (2023) 2671–2679.
[26] Y. Pan, X. Chen, L. Dong, et al., Chin. Chem. Lett. 32 (2021) 3895–3898.
[27] T. Zhu, N. Ren, X. Liu, et al., Angew. Chem. Int. Ed. 60 (2021) 8450–8454.
[28] L. Zhou, Z. Wang, L. Wang, et al., J. Am. Chem. Soc. 145 (2023) 28296–28306.
[29] W. Wang, T. Yang, Q. Zhang, et al., Anal. Chem. 95 (2023) 6279–6286.
[30] Q. Xu, Y. Zhang, M. Zhu, et al., Chem. Sci. 14 (2023) 4091–4101.
[31] C. Li, W. Tang, J. Feng, et al., Anal. Chim. Acta 1096 (2020) 148–158.
[32] Z. Zheng, S. Gong, J. Zhang, et al., Sens. Actuator B: Chem. 397 (2023) 134654.
[33] T. Han, Y. Sun, C. Zhao, et al., J. Med. Chem. 67 (2024) 4026–4035.
[34] P. Liu, B. Li, J. Zheng, et al., Sens. Actuator B: Chem. 329 (2021) 129147.
[35] Z. Xu, S. Liu, L. Xu, et al., Anal. Chim. Acta 1297 (2024) 342303.
[36] L. Ding, J. Jiang, L. Cheng, et al., ACS Appl. Bio Mater. 4 (2021) 3773–3785.